A Novel Pneumatic Soft Snake Robot Using Traveling-Wave Locomotion in Constrained Environments

Xinda Qi, Hongyang Shi, Thassyo Pinto, and Xiaobo Tan

***Abstract*—In this paper we propose a novel pneumatic soft snake robot which exploits traveling-wave motion to move in complex, constrained environments such as a pipeline. The robot is modular, with a unique pneumatic system design that requires the use of only four air channels regardless of the number of modules. The robot is 3D-printed, and thus low-cost and easy to build. Finite element modeling of the bending behavior of each module is conducted in ANSYS. The dynamic behavior of the robot, consisting of six modules, is further modeled in SOFA. In particular, it is found that the locomotion speed of the robot increases with the actuation pressure and decreases with the friction coefficient. Extensive experimental results on a snake robot prototype show good agreements with model predictions. The robot also demonstrates the capability of moving in constrained pipeline environments, including travelling in pipes of different diameters and challenging geometry such as a sharp elbow.**

***Index Terms*—Soft robot applications, additive manufacturing, snake robot, traveling-wave.**

I. Introduction

IN RECENT years, a number of robots have been developed by using inspirations from animals due to their advanced and robust locomotion capabilities. One class of such animals are snakes, which are capable of moving in most of the complex environments on earth. The slim body structure of the snakes enables them to travel in narrow, constrained environments. Snake-like robots are thus promising for applications such as pipeline inspection, search and rescue in rubbles, and minimally invasive surgeries.

Existing snake robots have predominantly adopted rigid modules. One classic snake robot utilized multiple motors to deform the rigid body, which demonstrated several different locomotion modes in traversing a complex terrain [1]–[3], climbing [4], and inspecting inside a pipeline [5]. Another multi-section snake robot achieved crawling on land and swimming in water [6]. Despite these progresses, there are some limitations for rigid snake robots. In particular, the size of a rigid snake robot is limited by the motors and complex mechanisms, which increases its difficulty in traversing a narrow environment.

To address the aforementioned concern, several soft snake robots driven by fluid power have been proposed. For example, soft snake robots with wheels were developed and their locomotion model was presented [7]–[11]. Soft snake robots can use the wave of its body to generate lateral undulation and side-winding locomotion. In addition, other than robots on wheels, soft snake robots can use the contact between the body and the environment to move forward by utilizing the anisotropic friction [12], [13]. Compared with a rigid snake robot, the size of a soft snake robot could be smaller and there is a large contact surface between the robot and environments. However, most of the reported soft snake robots require independent control of each module/section, with separate fluid channels/tubings for each module, which presents significant challenges in practical applications due to the resulting complexity in system hardware and control implementation.

In this work, a 3D-printed soft snake robot is proposed with a unique design for the pneumatic system and related control scheme to generate a traveling-wave using four air channels for the entire robot, regardless of the total number of modules for the robot. Unlike the casting approach used in most reported soft snake robots, 3D printing makes the fabrication simple and low-cost. Different from other lateral undulation soft snake robots that utilize wheels or anisotropic friction to move, the soft snake robot proposed in this paper uses two sides of the bending body, rather than the belly, to contact the constrained environment directly. The bending behavior of each module and the dynamic locomotion behavior of the robot are analyzed via finite element method (FEM) modeling with ANSYS and SOFA, respectively. In particular, among other things, the influence of friction contact on locomotion is studied in depth, and it is found that lower friction leads to faster locomotion speed. All modeling results are validated with extensive experiments on a six-module snake robot prototype. Additional experiments demonstrate robust locomotion of the snake robot in pipes of different diameters and geometry, including one with a sharp elbow, indicating the promise of the proposed robot in applications such as pipeline inspection.

The remainder of the paper is organized as follows. In Section II, the structure design and the fabrication method of the soft snake robot are described. The control scheme and the pressure actuation system are presented in Section III. The bending modes of the modular actuator are modeled, simulated, and experimentally validated in Section IV. In Section V, the modeling, simulation, and experimental study of locomotion

Manuscript received October 15, 2019; accepted January 6, 2020. Date of publication January 28, 2020; date of current version February 6, 2020. This letter was recommended for publication by Associate Editor R. MacCurdy and Editor K.-J. Cho upon evaluation of the reviewers' comments. This work was supported in part by an MSU Strategic Partnership under Grant 16-SPG-Full-3236. *(Corresponding author: Xinda Qi.)*

The authors are with the Department of Electrical and Computer Engineering, Michigan State University, East Lansing, MI 48824 USA (e-mail: qixinda@msu.edu; shihong1@egr.msu.edu; thassyo@msu.edu; xbtan@msu.edu).

This letter has supplementary downloadable material available at http://ieeexplore.ieee.org, provided by the authors.

Digital Object Identifier 10.1109/LRA.2020.2969923

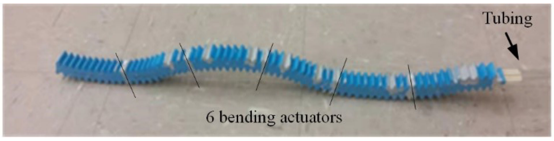

Fig. 1. A soft snake robot prototype developed in this work.

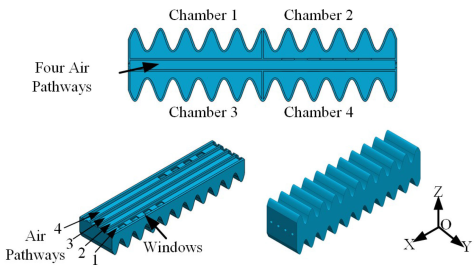

Fig. 2. Pneumatic actuator (modular section) of the robot body.

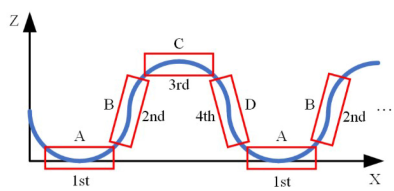

Fig. 3. Different bending modes of the actuators constitute a spatial serpentine wave.

behavior of the snake robot are discussed. Finally, concluding remarks are provided in Section VI.

II. Design and Fabrication of the Snake Robot

A. Robot Body Design

As a potential sensing platform for complex and constrained environments, the snake robot proposed in this paper has a simple and compact structure made of soft material. There are no rigid joints on the robot, minimizing the risk of failure. Also, without tubing on the sides of the body, the simple shape of the snake robot makes it easy to traverse a constrained environment.

The body of the soft snake, as illustrated by a prototype in Fig. 1, consists of multiple modular sections connected together (6 in the example here). Each section is a pneumatic bending actuator. The bending actuators share the same structure in general, but differ on the internal routing of air pathways.

For each pneumatic bending actuator, there are four separate air chambers and they are located on two sides of the robot's body, as shown in Fig. 2. The soft bellow surfaces of the snake body are used to amplify the deformation magnitude of the bending actuator and to improve the contact between the snake and complex working environments.

The four air chambers enable the actuator to have four different bending modes in the Z direction when different pairs of chambers are pressurized. The shapes of these bending modes are illustrated in Fig. 3. In particular, the actuator will bend in modes A and C when the chambers 1, 2 and chambers 3, 4 are actuated, respectively, and it will deform in modes B and D when chambers 1, 4 and chambers 2, 3 are actuated, respectively. This

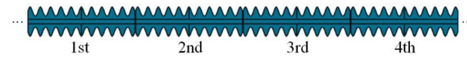

Fig. 4. One period of the snake robot's body.

TABLE I
Connection Between Air Paths and Chambers in Different Actuators in One Period of the Robot Body

	Chambers in different actuator			
Air Paths	1	2	3	4
1	3rd	2nd	1st	4th
2	2nd	1st	4th	3rd
3	1st	4th	3rd	2nd
4	4th	3rd	2nd	1st

design provides the basis for the traveling-wave generation in the spatial domain, because the four bending modes comprise one period of the serpentine wave, as shown in Fig. 3. The robot is comprised of the modular actuators linked together, with the corresponding air pathways designed such that modes A - D are concatenated as illustrated in Fig. 3. The robot can be made longer by adding modules, as long as the periodic sequencing of modes A - D is preserved. In this work, a robot consisting of six bending actuator modules is considered, to maintain at least two points of contact with the environment at any given time.

B. Pneumatic System Design

Different from previous works on soft snake robots, only four air paths are required in the proposed robot for the control of all the air chambers of the robot, regardless of the total number of bending actuator modules. This is important since it significantly reduces the complexity of hardware (valving, tubing) and control.

To prevent external tubing from interfering with the movement of the snake robot (especially in a constrained environment) and to minimize the total size of the robot, the air paths are designed to stay inside the snake body, as shown in Fig. 2. The four air paths are connected to the pneumatic source via tubing on the last bending actuator (the tail of the robot). The chambers and air paths are connected through several windows, which is the only difference between the four types of actuators, as shown in Fig. 2. Each air pathway is connected to one and only one of the chambers in each actuator.

The actuators in the snake body are classified into four types which are denoted as 1st, 2nd, 3rd, 4th in order, as shown in Fig. 4, and they constitute one period of the snake body. The linkage relationships between the air paths and the chambers in different types of actuators are shown in Table I.

A sinusoidal traveling-wave equation, which is used to approximate the movement of the robot, is characterized by:

$$z = A\sin(\omega t + kx) \tag{1}$$

which can be decomposed into the space domain and the time domain, separately:

$$\begin{cases} z = A\sin(\omega t + \theta_1), & \text{when } x \text{ is fixed} \\ z = A\sin(kx + \theta_2), & \text{when } t \text{ is fixed} \end{cases} \tag{2}$$

To illustrate the effect of the pneumatic system design of the robot, the snake robot's body configuration is studied discretely

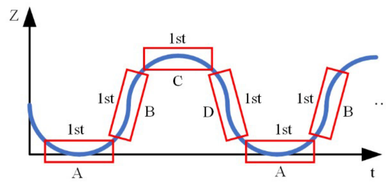

Fig. 5. Deformation modes of the 1st actuator constituting a time-domain serpentine wave.

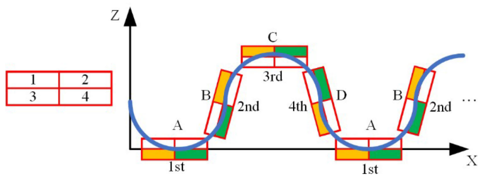

Fig. 6. Chambers linked to air path 1 (yellow) and air path 4 (green) in serpentine wave of the robot body.

when the 1st actuator is under the deformation mode A, B, C, D, which are the deformation modes at four representative times in one period of a traveling-wave, as shown in Fig. 5. The 1st actuator is under bending mode A when the air pathways 1 and 4 and the linked chambers are pressurized, as shown in Fig. 6. At the same time, the chambers 2 and 3 in the 2nd actuator are actuated, which make the 2nd actuator deform in mode B. As the Fig. 6 shows, the 3rd actuator and the 4th actuator deform in modes C and D under this condition, respectively. Thus, in the body length direction of the snake robot, the deformation modes A, B, C, D constitute one wavelength of the serpentine wave. Because of the periodicity of the snake robot modules, the rest of the body will continuously propagate the wave, which shows that the wave in space can be generated by the pneumatic system design under the condition that the 1st actuator has deformation mode A.

Similarly, it can be verified that when the 1st actuator deforms in modes B, C, D, the following actuators will deform accordingly in the phase-lagged modes to preserve a serpentine shape. This analysis shows that the pneumatic system design automatically decouples the traveling-wave generation into the spatial wave design, as shown in Fig. 3, and bending mode variations of one actuator in the time domain, as shown in Fig. 5. Such decoupling simplifies both the robot design and the control implementation. In addition, using just 4 air paths to control all the chambers in the long snake robot makes the system easy to fabricate and improves its operation robustness.

C. Prototyping and Fabrication

In prior work on soft robots, casting is a frequently used method for fabrication because the material used in casting is soft and results in large deformation [14]. However, the casting method requires complex and accurate operations and it is difficult to fabricate complex internal structures of a soft body. In this work we demonstrate the fabrication of the entire snake robot body, including its intricate air pathways, through 3D printing, which is another popular way to fabricate pneumatic soft actuator [15], [16]. The fused deposition modeling (FDM) 3D printer is selected to print the snake body because it is low-cost and it can print without support material by choosing proper parameters and designing a structure without large suspended areas. Although 3D printing with support material could have higher accuracy, unless the support material is soluble in solutions that do not affect the rest of the print, it would be extremely hard to remove the material and complete the fabrication, due to the complex structure inside the snake robot.

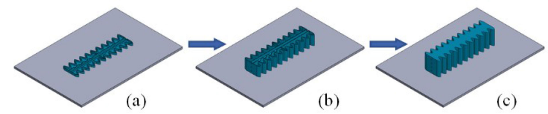

Fig. 7. 3D printing of the snake body: (a) Starting of the printing; (b) In printing; (c) Completion of the printing.

TABLE II
KEY PARAMETERS IN FDM 3D PRINTING

Parameters	Values
Nozzle diameter	0.4 mm
Extrusion width	0.45 mm
Extruder temperature	205 °C
Extruder multiplier	1.3
Printing speed	900 mm/min

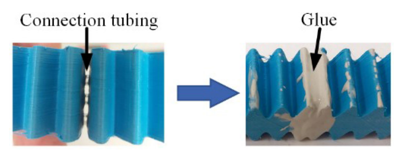

Fig. 8. Assembling process of different actuators of the snake body.

Filaflex 82A, a thermoplastic polyether-polyurethane elastomer (TPE) material, is used to print the body of the snake robot (i.e., the modular pneumatic actuators) because it has a sound balance between softness and elasticity. The dynamic requirement of the snake robot prevents the choice of a material that is too soft and exhibits excessive damping. The placement of the actuator and the printing procedure are shown in Fig. 7. Most of the major parts of the structure in the snake body (for example, the bellow walls on two sides of the body) can support themselves during the printing. However, there is still one upper surface that does not have enough support. So, the parameters including wall thickness, printing speed and extrusion multiplier are essential to avoiding under-extrusion for the last layers and preventing leakage problems. The 3D printer QIDI TECH I is used for fabrication and some key parameters used in 3D printing of the soft snake robot are shown in Table II.

The printer used in the fabrication has a build plate of 230 $\times$ 150 mm^2, which limits the length of the printed objects. Thus, the different actuators of the snake robot are printed separately and then connected in the designed order by short link tubing, which connects air paths of neighboring actuators, as shown in Fig. 8. Finally, the flexible glue Sikaflex is applied to fix and seal the connections.

III. Control Scheme and Actuation System

Control signals for the pressures in the four air channels are designed to achieve traveling-wave motion of the snake robot. One period of pressure signals is shown in Fig. 9, which are expressed as relative values with respect to the atmosphere.

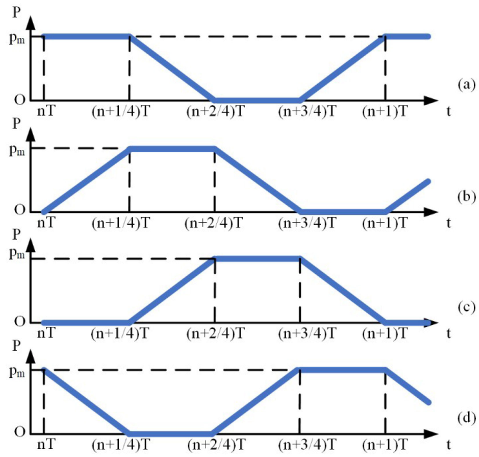

Fig. 9. Pressure control signals for four air paths: (a) Air path 1; (b) Air path 2; (c) Air path 3; (d) Air path 4. Here n = 0, 1, 2... and T is the time period.

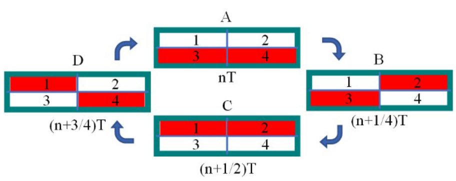

Fig. 10. Bending modes of 1st actuator in one period of traveling-wave.

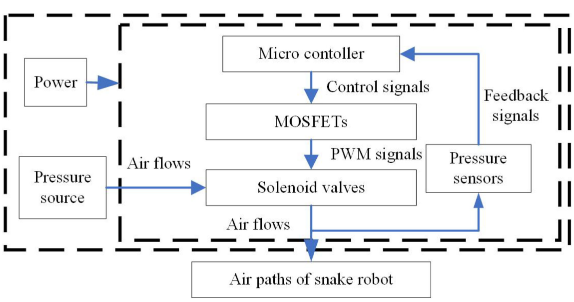

Fig. 11. Architecture of the pressure control board.

The bending modes of the 1st actuator when the air paths are actuated by the designed pressure control signals are shown in Fig. 10. At the time nT, (n + 1/4)T, (n + 2/4)T and (n + 3/4)T, the actuator shows bending modes A, B, C, D, respectively, which satisfies the serpentine wave designed in the time domain shown in Fig. 5. After the pressure values at the four discrete times are designed, linear interpolation is used to generate piece-wise linear pressure signals.

It is noticed that the pressure control signals have a quarter period phase lag sequentially from air path 1 to path 4, which influences the propagation direction of the traveling wave. If the control signals have a quarter period phase lead sequentially, the traveling wave will change its propagation direction to the opposite, which means that the snake robot can move forward and backward by altering the phase relationship between the pressure signals.

Fig. 11 shows the schematic of the pressure control system. The Arduino Mega is selected as the micro controller for the computation and communication of the system. PID controllers

TABLE III
PROPERTIES OF THE SOFT MATERIAL USED FOR THE ROBOT

Soft Material	**Filaflex 82A**
Density	1.12 g/cm^3
Stress at 20% elongation	2.5 MPa
Stress at 100% elongation	6 MPa
Stress at 200% elongation	10 MPa
Tensile strength	45 MPa

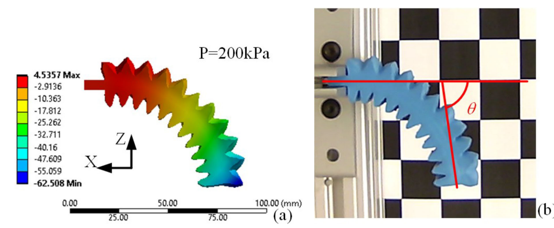

Fig. 12. The simulation and experiment of bending mode C when the applied pressure is 200 kPa : (a) the deformation in simulation, where the color indicates displacement in the Z-direction; (b) the deformation in experiment.

are used to track the desired pressure signals in a feedback system by modulating the PWM signals to four MOSFETs which are used for power amplification. The PWM signals are sent to solenoid valves (SMC VQ110U-5M) to control the airflow and the pressure in each of the four channels. Honeywell silicon pressure sensors “ASDXAVX100PGAA5” are used to provide the feedback.

IV. BENDING MODES ANALYSIS OF THE ACTUATOR

The finite element method (FEM) modeling and simulation are valuable tools for the analysis of soft robots [17], [18]. FEM modeling and simulation was conducted for static analysis of the four-chamber bending actuator module and a number of experiments were conducted to validate the FEM modeling and simulation.

The bending modes of the actuators are the basic deformation elements for generating traveling waves for the robot. Thus, FEM modeling and simulations were used to verify the bending modes of the actuators. The software ANSYS Workbench and the toolbox “Static Structural” were used, where the material parameters were derived from the technical sheet of the printing material; see Table III. Because of the relative low strain estimated for the actuator‘s deformation, a linear elastic model is used for the soft material, with Young’s modules of 12.5 MPa and Poisson ratio of 0.49.

In the four bending modes, modes A and C are symmetric of each other, and so are modes B and D. Fig. 12 shows the simulated bending mode C and its experimental counterpart, where the applied pressures (for chambers 1 and 2) were 200 kPa. The bending angle θ between the horizontal axis and the tangent line of the actuator’s mid-line at the right end is used to compare the deformations of mode C in simulations and experiments, as shown in Fig. 13. Fig. 14 shows the corresponding comparison between simulations and experiments for mode D, where the pressures were applied in chambers 1 and 4. Because the bending angle θ in mode D cannot describe the deformation efficiently, the displacement d of the right end of the actuator in the -Z direction is used to compare the simulations and experiments, as shown in Fig. 15.

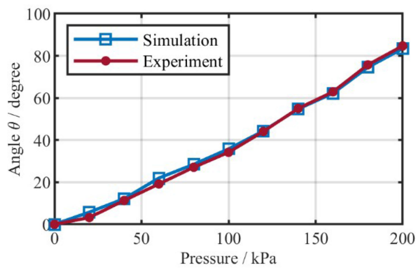

Fig. 13. The simulation and experimental results of the bending angle of the actuator in mode C.

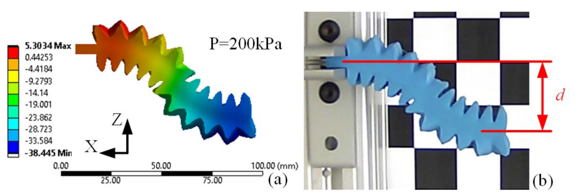

Fig. 14. The simulation and experiment of bending mode D when the applied pressure is 200 kPa : (a) the deformation in simulation, where the color indicates displacement in the Z-direction; (b) the deformation in the experiment.

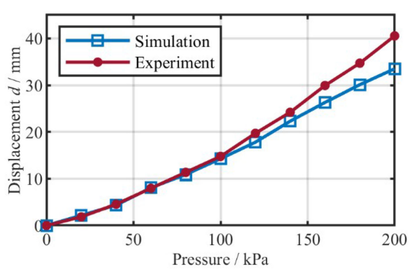

Fig. 15. The simulation and experiment results of the displacement in -Z direction of the actuator in mode D.

From the simulations and the experiments, it is verified that by applying pressure in specific chambers, the bending modes A, B, C, D can be generated as designed. Overall the FEM modeling is shown to capture well the behavior of the experimental prototype. In particular, the simulated bending angle shows good agreement with the experimental measurement. For the displacement curve, the discrepancy between the simulation and experimental results starts to show when the applied pressure is above 100 kPa. This might be attributed to the hyper-elasticity of the soft material.

V. Locomotion Analysis of the Snake Robot

FEM modeling and simulations were also conducted for dynamic analysis of the locomotion of the full snake robot in a constrained environment. In particular, a pipeline was considered for the constrained environment, given that an important potential application of soft snake robots is pipeline inspection. A number of experiments were conducted to validate the simulation and test the robot's performance and capability for traversing different pipeline environments.

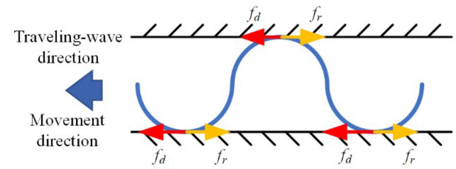

Fig. 16. Illustration of the soft snake robot locomotion under a traveling-wave.

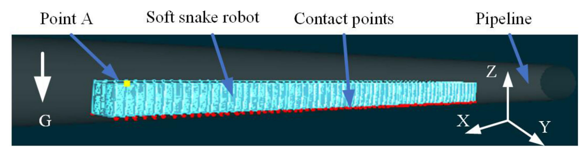

Fig. 17. Configuration of the SOFA simulation of the snake robot.

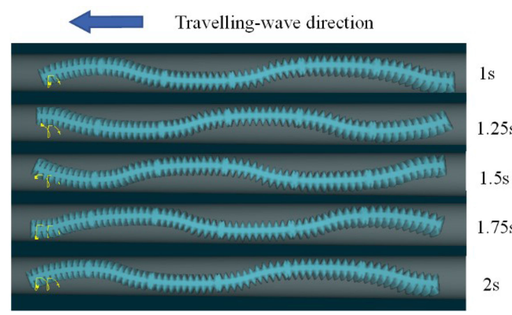

Fig. 18. The moving snake robot with a traveling-wave locomotion in the SOFA simulation, viewed from the -Z direction.

A. Dynamic Simulation of Robot Locomotion in Pipelines

The traveling-wave motion of the snake body generates the relative movement between the contact points of the snake robot and the environment, as discussed in the previous papers on traveling-wave locomotion [19], [20]. Thus, friction forces at the changing contact area of the snake robot drive the robot to move in the same direction of the traveling wave, as shown in Fig. 16. Like the dynamics of a rolling wheel, the driving force f_d and the resistance force f_r are both provided by friction.

FEM modeling of the dynamic locomotion for the soft snake robot has been conducted, which is able to accommodate complex collision and frictional contact. The FEM framework SOFA (Simulation Open Framework Architecture) has been used in dynamic simulation of soft robots [21], [22]. It is an efficient tool for physics simulation and meets the requirements of this work; in particular, it is amenable to dynamic FEM simulation and complex collision calculation. SOFA and the SOFT ROBOTS plugin were used for robot locomotion simulation in the constrained environment (pipeline). The basic configuration of SOFA simulation is shown in Fig. 17. The red points represent the contact nodes between the snake and the pipeline, and the yellow point is the node whose time-trajectory was studied.

Fig. 18 shows the traveling-wave motion of the snake robot within a 2-inch pipe, under the designed structure and pressure control signals, where the control signals' period was 1 s. The material properties and the gravity field were assigned, and the time step used in simulation was set to be 0.01 s. The yellow curve in Fig. 18 shows the trajectory of the studied point A,

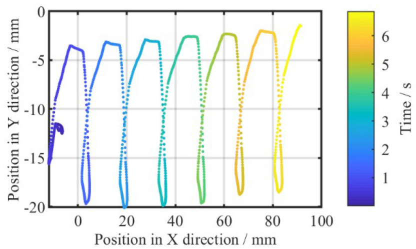

Fig. 19. The trajectory of point A in the XOY plane in the SOFA simulation.

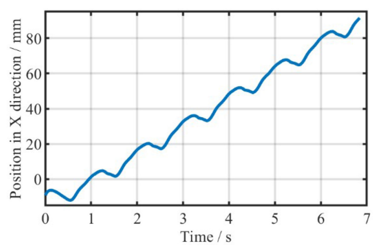

Fig. 20. The position of point A in the X direction in the SOFA simulation.

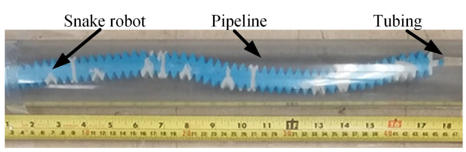

Fig. 21. Experiment setup for the snake robot locomotion.

which confirms that the robot moves in the same direction as the traveling-wave of the robot body.

From the dynamic simulation in SOFA, the trajectory data of point A is extracted, as shown in Fig. 19 and Fig. 20, when the friction coefficient between the robot and the pipeline is 0.65 and the maximum pressure of the control signal is 138 kPa (20 psi). The displacement per period of the snake robot is used as the average speed and is derived from the data in Fig. 20, which is about 16 mm/s when the period of traveling-wave is 1 s. These results suggest that SOFA can be used to simulate the dynamic locomotion and analyze the robot performance.

B. Experiments of Robot's Locomotion With Different Parameters

A number of experiments have been conducted to test the performance of the soft snake robot and to validate the SOFA analysis. The experiment setup for the snake robot's locomotion in a pipeline is shown in Fig. 21. A 2-inch clear PVC pipe was first selected as the constrained environment because of its small diameter and transparent body. The snake robot was placed in the pipeline in the same posture with the simulation so it could undulate in the horizontal plane. The speed of the robot was derived from the recorded video during the experiments.

A series of experiments was performed to verify the locomotion of the snake robot in pipelines and investigate the factors that influence the speed of the soft snake robot in the pipeline, with which the simulation results from SOFA were compared. The

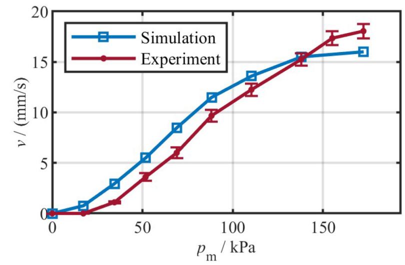

Fig. 22. The robot's speed in SOFA simulations and the experiments when friction coefficient μ is 0.65.

Fig. 23. Different inner surfaces of pipeline used in the experiments: (a) $\mu = 0.53$; (b) $\mu = 1.10$; (c) $\mu = 1.49$.

period T of signals and traveling-waves in all simulations and experiments was 1 s, which means that their frequency was 1 Hz. The first factor that influences the speed of the snake robot v is the maximum value p_m of the pressure signals. Fig. 22 shows the simulation results in SOFA and experiment results of the snake robot's locomotion. The friction coefficient μ between the clear PVC pipe and the soft material was measured to be 0.65, which was obtained as the ratio between the tensile force when pulling the robot along the pipe at a constant speed and the normal force between the robot and the pipe. The error bars of the experiment represent the means and the standard deviations of three runs of the experiments.

In the experiments, the speed of the robot increased from 0 to 18 mm/s when the maximum pressure p_m was increased from 0 to 172 kPa (25 psi). The corresponding simulation in SOFA showed that the robot's speed changes from 0 to 16 mm/s. The experiments also showed there was a dead zone in the relationships between p_m and v. Despite these minor discrepancies, overall the agreement between the simulation and experimental measurement is good.

Another important factor for speed is the friction coefficients between robot and pipelines, which were derived from the friction measurement tests. The relationships between v and p_m under different μ are shown in Fig. 24, Fig. 25 and Fig. 26, where a slippery polyethylene surface ($\mu = 0.53$), a paper surface ($\mu = 1.10$), and a metalized moisture-resistant polyester surface ($\mu = 1.49$), were used as the inner surface of the pipeline, respectively. Fig. 27 shows the relationship between μ and v in a 2-inch pipeline when the p_m was 138 kPa (20 psi) in SOFA simulations and the experiments.

From the simulations and the experiments, it can be seen that the speed of the soft snake robot decreases with an increasing friction coefficient for the contact between the robot and the environment. On the other hand, a higher friction coefficient is expected to result in higher payload capacity (before slip

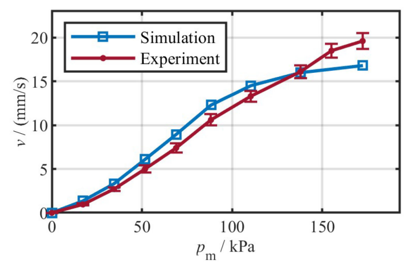

Fig. 24. The robot's speed in SOFA simulations and the experiments when friction coefficient μ is 0.53.

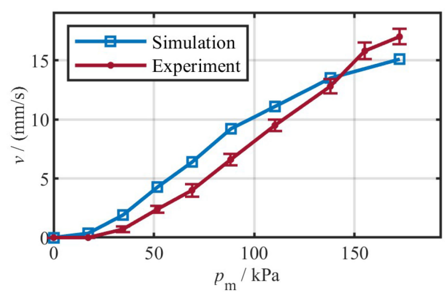

Fig. 25. The robot's speed in SOFA simulations and the experiments when friction coefficient μ is 1.10.

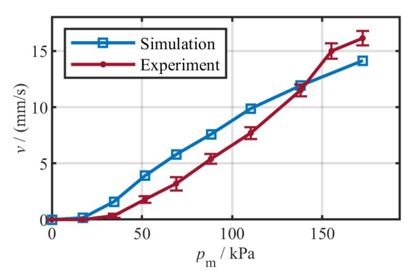

Fig. 26. The robot's speed in SOFA simulations and the experiments when friction coefficient μ is 1.49.

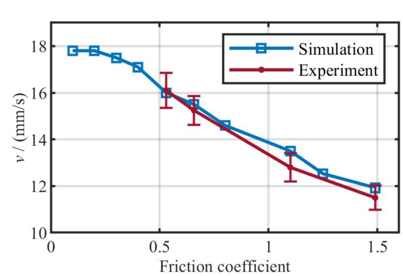

Fig. 27. The robot's speed in SOFA simulations and the experiments as a function of friction coefficient, when p_m is 138 kPa.

happens). Therefore, optimization of the frictional contact has to be taken into account multiple objectives.

C. Robot Locomotion in Complex Constrained Environments

The soft and compliant body of the snake robot makes it possible to adapt to different environments. To confirm that,

Fig. 28. The locomotion of the snake robot in a 1.625-inch pipeline.

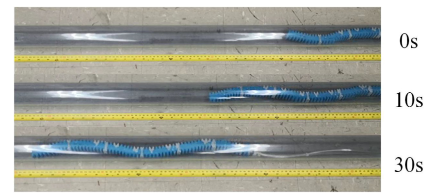

Fig. 29. The locomotion of the snake robot in a 2-inch pipeline.

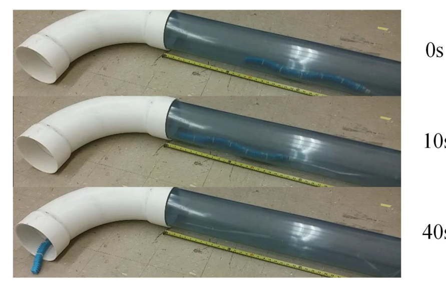

Fig. 30. The locomotion of the snake robot in a 6-inch pipeline.

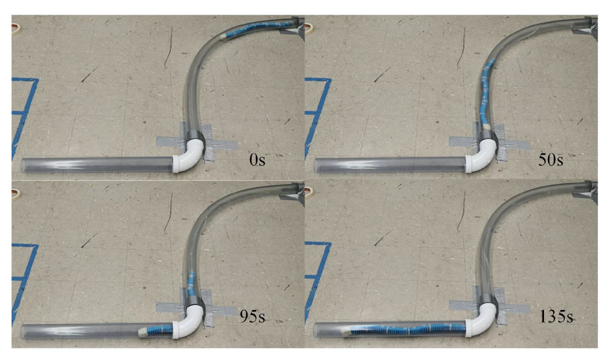

Fig. 31. The movement of the snake robot in a complex pipeline system of 2-inch pipelines.

we have performed experiments with pipelines of different diameters. Fig. 28, Fig. 29, and Fig. 30 show the locomotion of the snake robot in pipes of diameters of 1.625 inches, 2 inches, and 6 inches, respectively. The robot's average speeds in the straight parts of the three pipes were about 9 mm/s, 18 mm/s and 35 mm/s, respectively. These results show that the robot's speed increases with the diameter of the pipe, which can be explained by the fact that a larger pipe imposes less restriction on the robot, resulting in larger amplitude of the traveling-wave.

In addition, the soft snake robot was capable of passing the bending pipeline and even a sharp elbow, which revealed its robust locomotion in complex constrained environments and potential applications in pipeline inspection. Fig. 31 shows the locomotion of the snake robot in a complex pipeline system.

VI. Conclusion and Discussion

A novel pneumatic soft snake robot was proposed in this paper, which used a traveling-wave locomotion method moving in complex and constrained environments such as a pipeline system. The pneumatic system and the control scheme design enabled the snake robot to generate traveling-wave motion by only using four air paths, which simplified the body structure greatly and improve the snake robot's ability to move in constrained environments. In fabrication, 3D printing was used to build the whole body of the snake and made the robot robust, low-cost, lightweight and easy to build. FEM modeling and static structural simulation in ANSYS were conducted for bending mode verification, while dynamic simulation in SOFA was conducted for robot locomotion. Overall satisfactory agreement was achieved between model predictions and experimental measurements.

Extensive experiments were conducted to verify the robot's locomotion in pipelines and examine the relationship between the speed of the robot and the amplitude of pressure signals p_m under different frictional contact conditions. In a 2-inch PVC pipe, the speed of the snake robot using traveling locomotion reached 18 mm/s, for the maximum pressure of 172 kPa (25 psi) and the friction coefficient μ of 0.65. The speed of the robot increased with the maximum pressure, but decreased with an increasing friction coefficient (at least for the range of friction coefficient tested in this work). Furthermore, additional experiments showed that the proposed robot moved smoothly in pipes of different parameters and of complex geometry including sharp turns.

For future work, the design of the robot will be optimized based on FEM analysis using ANSYS and SOFA, the validity of which has been shown in this work. Factors to be optimized include geometry and dimensions of individual actuator modules, stiffness and frictional properties of the material, and the control signals. Multi-objective optimization will be pursued, to incorporate objectives in speed, payload capacity, power consumption, and size. We will also pursue integration of a compact pneumatic source, control board, and batteries with the robot to enable untethered operation and will study its ability to navigate inclined pipes and move on flat surfaces. We will further explore applications of the soft snake robot, such as inspection of gas distribution pipelines. These pipelines have relatively small diameters, often in the range of 2–4 inches, which makes it practically infeasible to deploy traditional rigid robots efficiently.

Acknowledgment

The authors would like to thank Mohammed Al-Rubaiai and Dr. Cody Pinger for the help on 3D printing.

References

[1] C. Wright *et al.*, "Design of a modular snake robot," in *Proc. IEEE/RSJ Int. Conf. Intell. Robots Syst.*, Oct. 2007, pp. 2609–2614.

[2] K. Lipkin *et al.*, "Differentiable and piecewise differentiable gaits for snake robots," in *Proc. IEEE/RSJ Int. Conf. Intell. Robots Syst.*, Oct. 2007, pp. 1864–1869.

[3] C. Wright *et al.*, "Design and architecture of the unified modular snake robot," in *Proc. IEEE Int. Conf. Robot. Autom.*, May 2012, pp. 4347–4354.

[4] J. Whitman, N. Zevallos, M. Travers, and H. Choset, "Snake robot Urban search after the 2017 Mexico City earthquake," in *Proc. IEEE Int. Symp. Saf., Secur. Rescue Robot.*, Aug. 2018, Art. no. 18098780.

[5] D. Rollinson and H. Choset, "Pipe network locomotion with a snake robot," *J. Field Robot.*, vol. 33, no. 3, pp. 322–336, 2016.

[6] A. Crespi and A. J. Ijspeert, "Amphibot II: An amphibious snake robot that crawls and swims using a central pattern generator," in *Proc. 9th Int. Conf. Climbing Walking Robots*, 2006, pp. 19–27.

[7] C. D. Onal and D. Rus, "Autonomous undulatory serpentine locomotion utilizing body dynamics of a fluidic soft robot," *Bioinspiration Biomimetics*, vol. 8, no. 2, Mar. 2013, Art. no. 026003.

[8] C. D. Onal and D. Rus, "A modular approach to soft robots," in *Proc. 4th IEEE RAS EMBS Int. Conf. Biomed. Robot. Biomechatronics*, Jun. 2012, pp. 1038–1045.

[9] M. Luo *et al.*, "Slithering towards autonomy: A self-contained soft robotic snake platform with integrated curvature sensing," *Bioinspiration Biomimetics*, vol. 10, no. 5, Sep. 2015, Art. no. 055001.

[10] M. Luo, W. Tao, F. Chen, T. K. Khuu, S. Ozel, and C. D. Onal, "Design improvements and dynamic characterization on fluidic elastomer actuators for a soft robotic snake," in *Proc. IEEE Int. Conf. Technologies Practical Robot Appl.*, Apr. 2014, pp. 1–6.

[11] M. Luo *et al.*, "Orisnake: Design, fabrication, and experimental analysis of a 3-D origami snake robot," *IEEE Robot. Autom. Lett.*, vol. 3, no. 3, pp. 1993–1999, Jul. 2018.

[12] C. Branyan and Y. Menğüç, "Soft snake robots: Investigating the effects of gait parameters on locomotion in complex terrains," in *Proc. IEEE/RSJ Int. Conf. Intell. Robots Syst.*, Oct. 2018, Art. no. 18372928.

[13] C. Branyan *et al.*, "Soft snake robots: Mechanical design and geometric gait implementation," in *Proc. IEEE Int. Conf. Robot. Biomimetics*, Dec. 2017, pp. 282–289.

[14] K. C. Galloway, P. Polygerinos, C. J. Walsh, and R. J. Wood, "Mechanically programmable bend radius for fiber-reinforced soft actuators," in *Proc. 16th Int. Conf. Adv. Robot.*, Nov. 2013, Art. no. 14161478.

[15] O. D. Yirmibesoglu *et al.*, "Direct 3D printing of silicone elastomer soft robots and their performance comparison with molded counterparts," in *Proc. IEEE Int. Conf. Soft Robot.*, Apr. 2018, pp. 295–302.

[16] B. N. Peele, T. J. Wallin, H. Zhao, and R. F. Shepherd, "3D printing antagonistic systems of artificial muscle using projection stereolithography," *Bioinspiration Biomimetics*, vol. 10, no. 5, Sep. 2015, Art. no. 055003.

[17] P. Polygerinos *et al.*, "Modeling of soft fiber-reinforced bending actuators," *IEEE Trans. Robot.*, vol. 31, no. 3, pp. 778–789, Jun. 2015.

[18] K. Suzumori, S. Endo, T. Kanda, N. Kato, and H. Suzuki, "A bending pneumatic rubber actuator realizing soft-bodied manta swimming robot," in *Proc. IEEE Int. Conf. Robot. Autom.*, Apr. 2007, pp. 4975–4980.

[19] D. Zarrouk, M. Mann, N. Degani, T. Yehuda, N. Jarbi, and A. Hess, "Single actuator wave-like robot (SAW): Design, modeling, and experiments," *Bioinspiration Biomimetics*, vol. 11, no. 4, Jul. 2016, Art. no. 046004.

[20] L. Chen, S. Ma, Y. Wang, B. Li, and D. Duan, "Design and modelling of a snake robot in traveling wave locomotion," *Mechanism Mach. Theory*, vol. 42, no. 12, pp. 1632–1642, 2007.

[21] J. Allard *et al.*, "SOFA - an open source framework for medical simulation," *Studies Health Technol. Informat.*, vol. 125, pp. 13–8, Feb. 2007.

[22] C. Duriez and T. Bieze, "Soft robot modeling, simulation and control in real-time," *Soft Robotics: Trends, Applications and Challenges*. Cham: Springer, 2017, pp. 103–109.